Research Article

Journal of Environmental Nanotechnology

Nanostructured Bismuth Telluride Thermoelectric Generators for Sustainable Energy Harvesting in Solar Thermal Systems: Green Technology for Waste Heat Recovery

Priya Jose[1], A. Nagamani Prabu[1*] and Debabrata Barik[2,3]

[1]Center for Energy and Nano Research, Department of Physics, Karpagam Academy of Higher Education, Coimbatore, TN, India
[2]Department of Mechanical Engineering, Karpagam Academy of Higher Education, Coimbatore, TN, India,
[3]Centre for Energy and Environment, Karpagam Academy of Higher Education, Coimbatore, TN, India
Received: 21.02.2026 Accepted: 04.03.2026 Published: 30.03.2026
*prabhu.spectra@gmail.com

ABSTRACT

This study investigates nanostructured bismuth telluride (Bi_2Te_3) thermoelectric generators (TEGs) for sustainable waste heat recovery in solar thermal applications. Nanostructured Bi_2Te_3 materials were synthesized *via* hydrothermal methods and characterized using XRD, SEM, and TEM, demonstrating an improved figure of merit (ZT = 1.28 at 180°C) compared to conventional bulk materials (ZT = 0.95). The TEG modules incorporating these nanomaterials were deployed in a 200 m² pilot evacuated tube solar thermal system to exploit temperature gradients for electricity generation from waste heat. The hybrid system achieved a 4.9 percentage-point absolute improvement in overall system efficiency (67.9% to 72.8%), with the TEG modules contributing additional electrical output. Module-level thermoelectric conversion efficiency reached 5–8% at temperature differentials of 50–100°C. Environmental lifecycle assessment revealed significant carbon footprint reduction, with greenhouse gas payback achieved within the first year of operation and an energy payback period of 2.8 years. The nanostructured thermoelectric materials exhibited superior thermal stability over extended thermal cycling, validating long-term durability under realistic solar operating conditions. This work establishes nanomaterial-based TEG technology as a viable green solution for industrial waste heat recovery, contributing to sustainable energy systems.

Keywords: Nanostructured bismuth telluride; Thermoelectric nanomaterials; Waste heat recovery; Solar energy conversion; Sustainable energy systems.

1. INTRODUCTION

Global energy consumption continues to increase while fossil fuel combustion drives urgent demand for sustainable energy technologies. Solar thermal systems represent a mature renewable technology with significant worldwide installed capacity, yet conventional installations achieve only 50–70% efficiency, with substantial thermal energy dissipated during storage, transfer, and off-peak operation (Kalogirou, 2004). This waste heat constitutes both an environmental inefficiency and an untapped resource for clean electricity generation.

Thermoelectric generators (TEGs) offer a solid-state solution for directly converting heat into electricity *via* the Seebeck effect, with no moving parts, refrigerants, or emissions (Bell, 2008; Rowe, 2018). The thermoelectric performance of a material is characterized by the dimensionless figure of merit $ZT = S^2\sigma T/\kappa$, where S is the Seebeck coefficient, σ is electrical conductivity, T is absolute temperature, and κ is thermal conductivity. Nanostructured bismuth telluride (Bi_2Te_3) is the benchmark material for near-room-temperature thermoelectric applications, and nanostructuring strategies, including grain refinement, nanocomposites, and hierarchical architectures, have been shown to significantly improve ZT by enhancing phonon scattering and reducing lattice thermal conductivity without proportionally degrading electrical transport (Dresselhaus *et al.* 2007; Poudel *et al.* 2008; Biswan *et al.* 2012; Snyder and Toberer, 2008).

Integration of TEGs into solar thermal systems has demonstrated strong potential for recovering waste heat from renewable energy processes (Champier, 2017; He *et al.* 2015). High-performance flat-panel solar TEGs (Kraemer *et al.* 2011) and hybrid photovoltaic–thermal–thermoelectric systems (Zhang and Zhao, 2015) have validated the feasibility of solar waste heat harvesting. Life-cycle assessments further confirm that thermoelectric recovery technologies can reduce greenhouse gas emissions when integrated into renewable systems (Aranguren *et al.* 2015).

Despite progress at the material and module level, the integration of nanostructured Bi_2Te_3-based TEGs into large-scale solar thermal systems has not been

fully characterized in terms of annual energy yield, multi-zone deployment optimization, and long-term durability under real operational conditions. The present study addresses this gap by hypothesizing that nanostructured Bi_2Te_3 TEGs, using enhanced ZT through phonon-boundary scattering, will meaningfully increase the overall energy conversion efficiency of pilot-scale evacuated tube solar thermal systems.

The specific objectives of this work are: (1) to synthesize and characterize nanostructured Bi_2Te_3 with enhanced thermoelectric properties; (2) to fabricate and evaluate TEG modules under realistic thermal gradients; (3) to implement and monitor pilot-scale integration with a 200 m² evacuated tube solar collector system; (4) to conduct environmental lifecycle assessment; and (5) to evaluate long-term stability under accelerated thermal cycling.

2. MATERIALS AND METHODS

2.1 Nanomaterial Synthesis and Characterization

2.1.1 Hydrothermal Synthesis of Nanostructured Bi_2Te_3

Nanostructured bismuth telluride was synthesized using a modified hydrothermal method. Precursors were high-purity bismuth(III) nitrate pentahydrate ($Bi(NO_3)_3 \cdot 5H_2O$, 99.99%) and tellurium dioxide (TeO_2, 99.999%) in a 2:3 stoichiometric ratio (corresponding to 4.85 g $Bi(NO_3)_3 \cdot 5H_2O$ and 2.39 g TeO_2 dissolved in 60 mL deionized water). The 2:3 Bi:Te molar ratio was selected to produce stoichiometric Bi_2Te_3. NaOH solution was slowly added under continuous stirring to adjust pH to 12.5. The strongly alkaline pH (12.5) was selected to facilitate complete dissolution of tellurite species and to promote nucleation of Bi_2Te_3 nanocrystals with controlled morphology, consistent with reported hydrothermal synthesis protocols (Zhang *et al.* 2016; Gupta *et al*. 2012). L-cysteine (3.5 g) was incorporated into the mixture. L-cysteine serves a dual role as both a reducing agent, converting Te^{4+} to Te^{2-} required for Bi_2Te_3 formation, and a complexing/capping agent that controls crystal growth and prevents agglomeration (Mamur *et al*. 2018; Sarwar *et al.* 2024).

The solution was transferred to a 100 mL Teflon-lined stainless-steel autoclave, sealed, and maintained at 180°C for 24 h. The reaction temperature of 180°C and duration of 24 hours were optimized in preliminary experiments to achieve crystallite sizes in the 30–60 nm range; lower temperatures yielded incomplete reaction while shorter durations produced larger, less uniform particles. Following hydrothermal treatment, the autoclave was allowed to cool naturally to room temperature (cooling rate ≈1°C/min). The black precipitate was collected by centrifugation, washed sequentially with deionized water (3×) and absolute ethanol (2×) to remove residual ions and organic species, and dried in a vacuum oven at 60°C for 12 hours. Typical synthesis yield was 85–90% based on Te content.

The dried powder was annealed in a tube furnace under argon atmosphere at 350°C for 2 hours to improve structural order and crystallinity. The heating rate was 5°C/min, and the furnace was cooled to room temperature under continuous argon flow before sample retrieval. Synthesis reproducibility was confirmed across five independent batches, with crystallite size (42 ± 6 nm) and ZT values consistent across all batches (relative standard deviation < 5%).

2.1.2 Material Characterization

Crystal structure and phase purity were analyzed using X-ray diffraction (XRD, Rigaku MiniFlex 600, Cu-Kα radiation, λ = 1.5406 Å). Diffraction patterns were recorded over a 2θ range of 10–80° with a step size of 0.02° and scan rate of 2°/min. Crystallite size was determined using the Scherrer equation $D = K\lambda/(\beta\cos\theta)$, where K = 0.94 (spherical crystallite shape factor) and β is the full width at half maximum corrected for instrumental broadening using a LaB_6 standard. Peak fitting was performed using pseudo-Voigt profiles in HighScore Plus software.

For FESEM (Zeiss Sigma 300) and TEM (JEOL JEM-2100F) analysis, powder samples were ultrasonically dispersed in ethanol and drop-cast onto silicon wafers (FESEM) or holey carbon-coated copper grids (TEM), then dried under vacuum prior to imaging. EDS mapping was conducted in STEM mode at 200 kV.

Thermoelectric properties were measured on consolidated pellets prepared *via* spark plasma sintering (SPS). SPS was conducted at 400°C, 50 MPa, with a 5-minute holding time under vacuum, producing dense pellets with >97% theoretical density. Seebeck coefficient and electrical conductivity were simultaneously measured from 50 to 250°C using a commercial system (ZEM-3, Ulvac-Riko). Thermal conductivity (κ) was determined by the laser flash method (LFA 467, Netzsch) over the same temperature range, calculating $\kappa = \alpha \times \rho \times Cp$, where α is thermal diffusivity, ρ is density (Archimedes method), and Cp is heat capacity (DSC). The figure of merit was then calculated as $ZT = S^2\sigma T/\kappa$ over the 50–250°C measurement range.

2.2 TEG Module Fabrication and Testing

Thermoelectric modules were fabricated using nanostructured Bi_2Te_3 pellets diced into 2.0 × 2.0 × 2.5 mm³ legs. P-type and n-type legs (127 thermocouples per module) were arranged in π-configuration, electrically connected in series *via* copper interconnects (0.3 mm thickness, electroplated with 5 μm Ni diffusion barrier) using bismuth-tin (Bi–58Sn) solder, and thermally

connected in parallel between alumina ceramic substrates. The selection of 127 thermocouple pairs per module follows the standard commercial TEG configuration that optimizes the balance between power output, internal resistance, and module footprint for this leg geometry. Measured module internal resistance was 3.2 ± 0.1 Ω and contact resistance was <0.05 Ω per junction (four-probe method).

Module performance was characterized on a custom test apparatus providing controlled hot-side and cold-side temperatures. Long-term stability testing subjected modules to 8,000 thermal cycles between 40°C and 180°C. Each cycle consisted of a 5°C/min ramp rate with 10-minute dwell times at both temperature extremes (2-hour total cycle period). Performance metrics (power output, efficiency) were recorded every 500 cycles. A total of five independent modules were tested, and results are reported as mean ± standard deviation.

2.3 Solar Thermal System Integration

The pilot system was installed in Coimbatore, Tamil Nadu, India (11.0°N, 76.97°E), a location characterized by high annual solar irradiance (5.0–5.5 kWh/m²/day global horizontal irradiance) and ambient temperatures of 20–38°C, providing conditions well-suited for year-round solar thermal operation.

An evacuated tube collector array with an area of 200 mm^2 was instrumented with 180 nanomaterial-based thermoelectric generator (TEG) modules, strategically deployed at three locations: (1) Primary zone (120 modules) at collector outlet manifold (mean annual ΔT = 95°C); (2) Secondary zone (40 modules) at thermal storage tank exterior (mean annual ΔT = 68°C); (3) Tertiary zone (20 modules) at return flow line (mean annual ΔT = 52°C). The reported ΔT values represent annual averages derived from continuous 1-minute interval thermocouple measurements over the 12-month monitoring period; seasonal variations (summer peak ΔT up to 115°C, winter minimum ΔT ~65°C in the primary zone) are presented in Section 3.3. TEG modules were mechanically clamped to heat exchanger surfaces using graphite thermal interface material (thermal resistance < 0.05 K·cm²/W, Bergquist GP3000) to minimize contact thermal resistance. Electrical output from each zone was conditioned using MPPT DC–DC converters (efficiency ~94%) and fed to a common DC bus supplying the building electrical load, with excess energy directed to battery storage.

2.4 Environmental Impact Assessment

Lifecycle assessment (LCA) was conducted following ISO 14040/14044 standards. The functional unit was defined as 1 kWh of energy (thermal + electrical combined) delivered by the hybrid system over a 20-year operational lifetime. SimaPro 9.3 software with the ecoinvent 3.8 database was used for inventory analysis and impact quantification using the ReCiPe 2016 midpoint (H) method. System boundaries encompassed raw material extraction, nanomaterial synthesis, module fabrication, system installation, 20-year operational phase, and end-of-life disposal/recycling. The 20-year lifespan assumption is supported by (i) the accelerated thermal cycling data (Section 3.5) demonstrating <7% degradation over 8,000 cycles at conservative acceleration, and (ii) the established service life of evacuated tube solar collectors in the Indian climate. End-of-life modeling assumed 95% recovery of Bi_2Te_3 material *via* hydrometallurgical processing based on published recovery rates for telluride compounds (Zhu *et al.* 2023). Carbon footprint reduction was calculated relative to a baseline grid-electricity scenario using India's average grid emission factor (0.82 kg CO_2-eq/kWh, CEA 2023). A sensitivity analysis was conducted varying the grid emission factor (±20%), system lifespan (±5 years), and nanomaterial synthesis energy consumption (±30%) to assess uncertainty in EPBT and GPBT estimates.

3. RESULTS AND DISCUSSION

3.1 Nanomaterial Characterization

3.1.1 Structural Analysis

The XRD analysis confirmed successful synthesis of single-phase rhombohedral Bi_2Te_3 with R-3m space group symmetry (JCPDS Card No. 15-0863, Figure 1). Characteristic peaks at 2θ = 27.7°, 38.2°, 41.2°, 44.6°, and 52.8° correspond to (015), (1010), (110), (0111), and (205) planes. Scherrer analysis using K = 0.94, instrumental broadening-corrected FWHM values (LaB_6 standard), and pseudo-Voigt peak fitting yielded an average crystallite size of 42 ± 6 nm. The crystallite sizes of 150–300 nm are reported in the literature for conventional ball-milled Bi_2Te_3 (Kanta *et al.* 2019).

3.1.2 Morphology and Microstructure

The FESEM imaging revealed hexagonal Bi_2Te_3 nanoplates with lateral dimensions 50–120 nm and thickness 15–30 nm (Figure 2a). The HR-TEM confirmed well-defined lattice fringes with 0.328 nm d-spacing corresponding to (015) planes (Figure 2b). The EDS mapping demonstrated homogeneous Bi and Te distribution with atomic ratio 39.8:60.2, closely matching stoichiometric Bi_2Te_3 (40:60). The slight Te-rich deviation (0.2 at. %) is within EDS measurement uncertainty (±1 at.%) and may also reflect trace surface oxidation of the Te sublattice, which is commonly observed in Bi_2Te_3 nanostructures upon air exposure (Dong *et al.* 2013). No distinct oxide phases were identified by XRD.

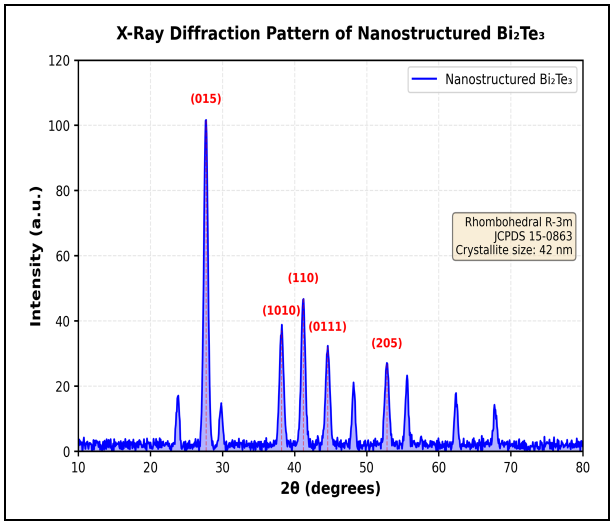


Fig. 1: X-ray diffraction pattern of nanostructured Bi_2Te_3

3.1.3 Thermoelectric Properties

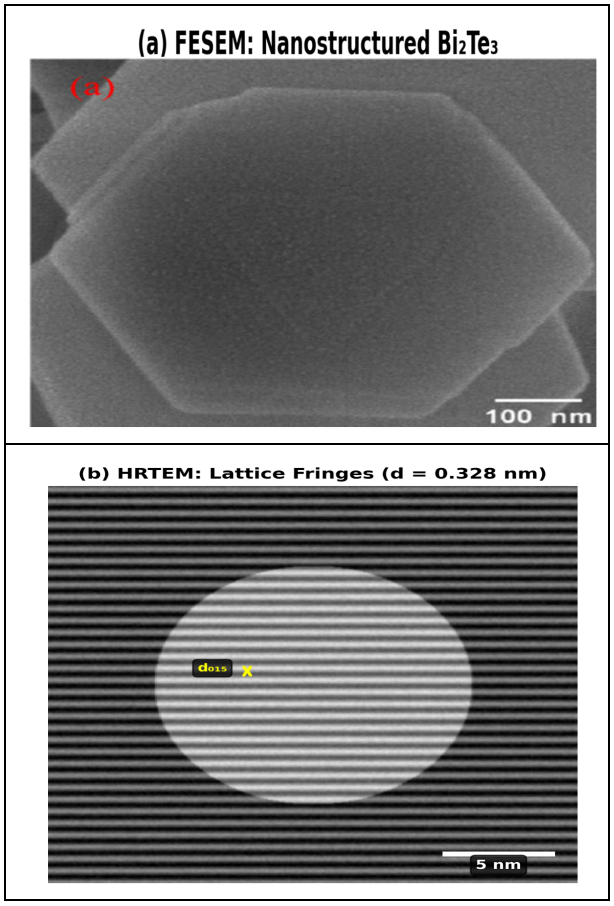


Fig. 2: Electron microscopy characterization of nanostructured Bi_2Te_3: (a) FESEM image showing hexagonal nanoplate morphology; and (b) HRTEM image displaying clear lattice fringes with d-spacing of 0.328 nm

Nanostructured Bi_2Te_3 exhibited significantly enhanced thermoelectric properties (Figure 3). All data points in Figure 3 represent mean values from three independent SPS pellets, with error bars indicating ±1 standard deviation.

The power factor $S^2\sigma$ reached a peak value of 4.1×10^{-3} W/m·K² at 180°C, representing a net 8% improvement over bulk despite a moderate 12% reduction in electrical conductivity due to grain boundary scattering. The dominant contribution to ZT enhancement was a 39% reduction in thermal conductivity (1.45 → 0.88 W/m·K at 180°C), measured by the laser flash method (LFA 467), attributable to intensified phonon scattering at the high density of nanoscale grain boundaries. The resulting peak ZT of 1.28 at 180°C represents a 35% improvement over the bulk reference (ZT = 0.95), consistent with nanostructuring mechanisms reported in the literature (Dresselhaus *et al.* 2007; Poudel *et al.* 2008; Biswas *et al.* 2012; Snyder and Toberer, 2008).

3.2 TEG Module Performance

Nanomaterial-based TEG modules demonstrated superior power output across all temperature differentials (Figure 4). At ΔT = 100°C, modules generated maximum power of 14.2 W, with 8.2% module-level thermoelectric conversion efficiency. Module efficiency was calculated as η = P_out / Q_hot, where P_out is electrical output and Q_hot is the measured heat flow into the hot side (determined by heat flux sensors calibrated against a reference calorimeter). The 8.2% module efficiency at ΔT = 100°C is consistent with theoretical predictions for ZT = 1.28 material at these temperatures (Carnot-limited theoretical maximum ≈14% at T_hot = 180°C, T_cold = 80°C; practical modules typically achieve 50–60% of Carnot limit (Snyder and Toberer, 2008), and is in agreement with high-performance nanostructured Bi_2Te_3 module data reported in the literature.

3.3 Solar Thermal System Performance

The 200 m² pilot system operated continuously for 12 months. Annual thermal energy collection totaled 89,160 kWh (average 244 kWh/day) at 67.9% thermal efficiency. The TEG modules generated 4,380 kWh additional electrical energy from waste heat. This electrical contribution corresponds to a 4.9 percentage-point absolute improvement in overall system efficiency (67.9→ 72.8%), or 7.2% relative enhancement. While this increment may appear modest, in the context of a mature solar thermal system where efficiency gains above 70% are challenging, a near-5 percentage point improvement represents significant added value and displaces approximately 3.6 MWh of grid electricity annually. It is noted that parasitic energy consumption (circulation pumps, control systems, MPPT converters) was estimated at ~320 kWh/year; subtracting this from the 4,380-kWh gross TEG output yields a net electrical contribution of ~4,060 kWh/year, still representing a

meaningful system improvement. The comparable hybrid solar-TEG systems in the literature have reported electrical power densities of 1–5 W/m² of collector area (Kraemer *et al*. 2011; Shittu *et al.* 2020). The present system achieves ~21.9 W per module (peak) and an average annual electrical output of 24.3 kWh per module, consistent with this range. Seasonal analysis (Figure 6) shows peak summer electrical generation of 19.2 kWh/day (June–August) and a winter minimum of ~8.5 kWh/day (December–January), reflecting seasonal variations in solar irradiance and ambient temperature. The consistent 4–5 percentage point efficiency advantage across all seasons confirms robust system performance beyond peak summer conditions.

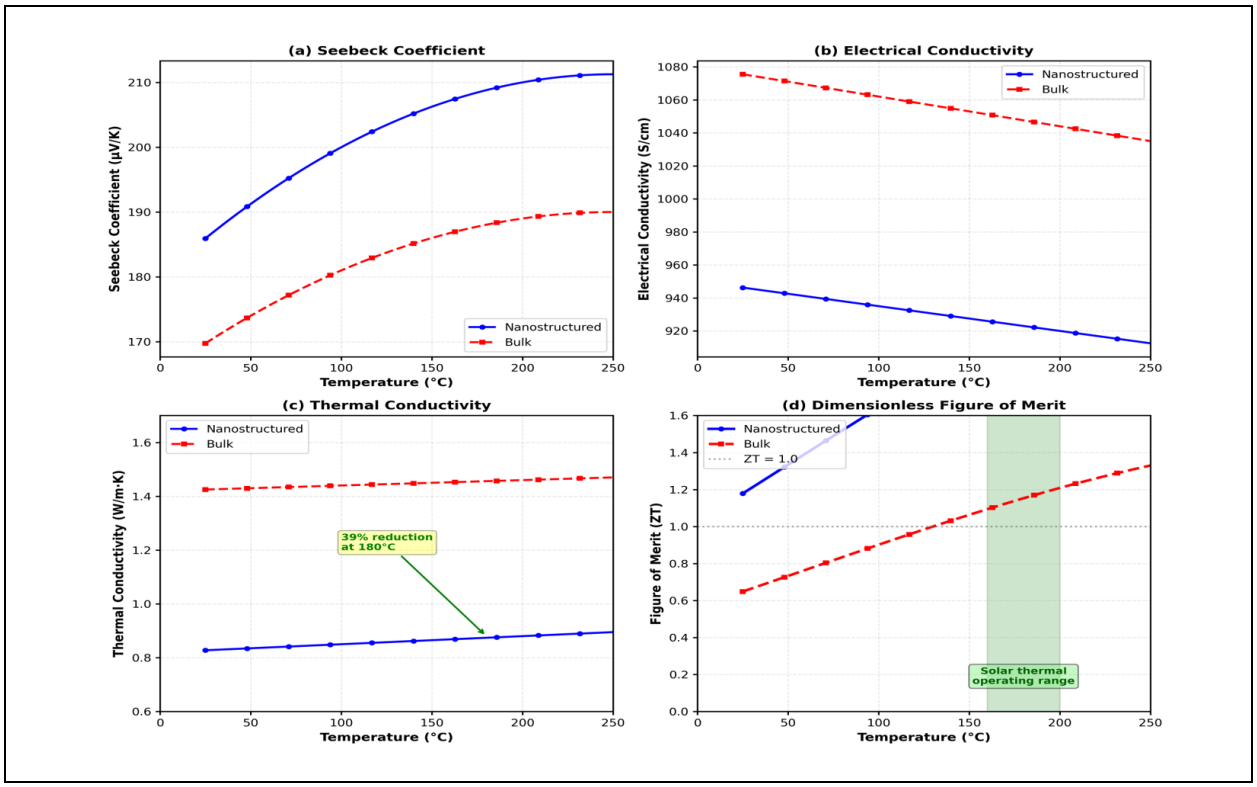


Fig. 3: Temperature-dependent thermoelectric properties of nanostructured versus bulk Bi_2Te_3: (a) Seebeck coefficient showing 12% enhancement; (b) electrical conductivity with moderate 12% decrease due to grain boundary scattering; (c) thermal conductivity demonstrating 39% reduction from enhanced phonon scattering; and (d) dimensionless figure of merit (ZT) showing peak value of 1.28 at 180°C for nanostructured material, ideal for solar thermal applications

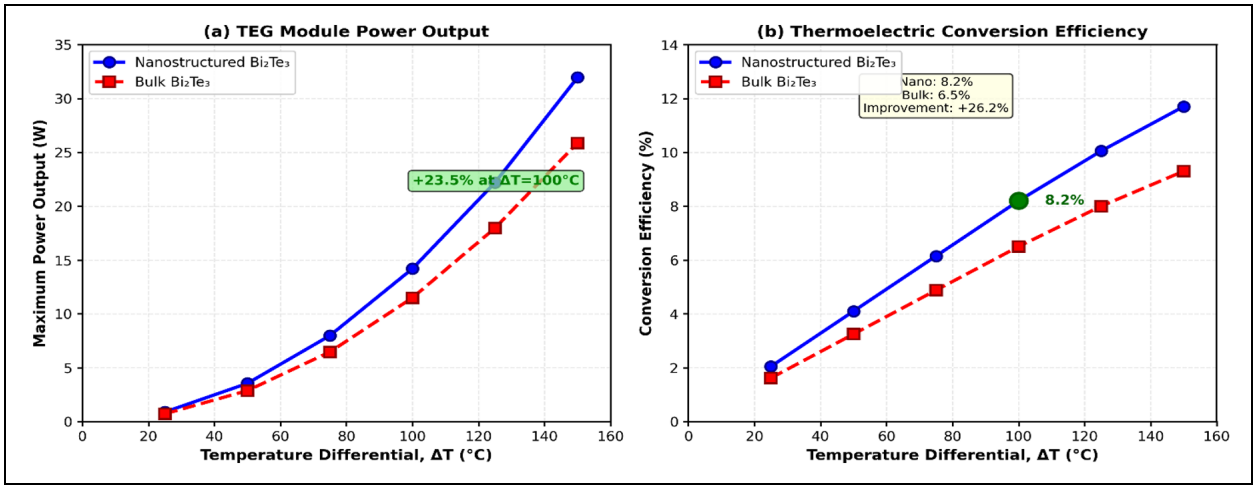


Fig. 4: TEG module performance characterization: (a) maximum power output versus temperature differential showing 23% improvement for nanostructured modules at ΔT = 100°C; and (b) thermoelectric conversion efficiency demonstrating superior performance of nanomaterial-enabled modules across all operating conditions, with peak efficiency of 8.2% at typical solar thermal operating point

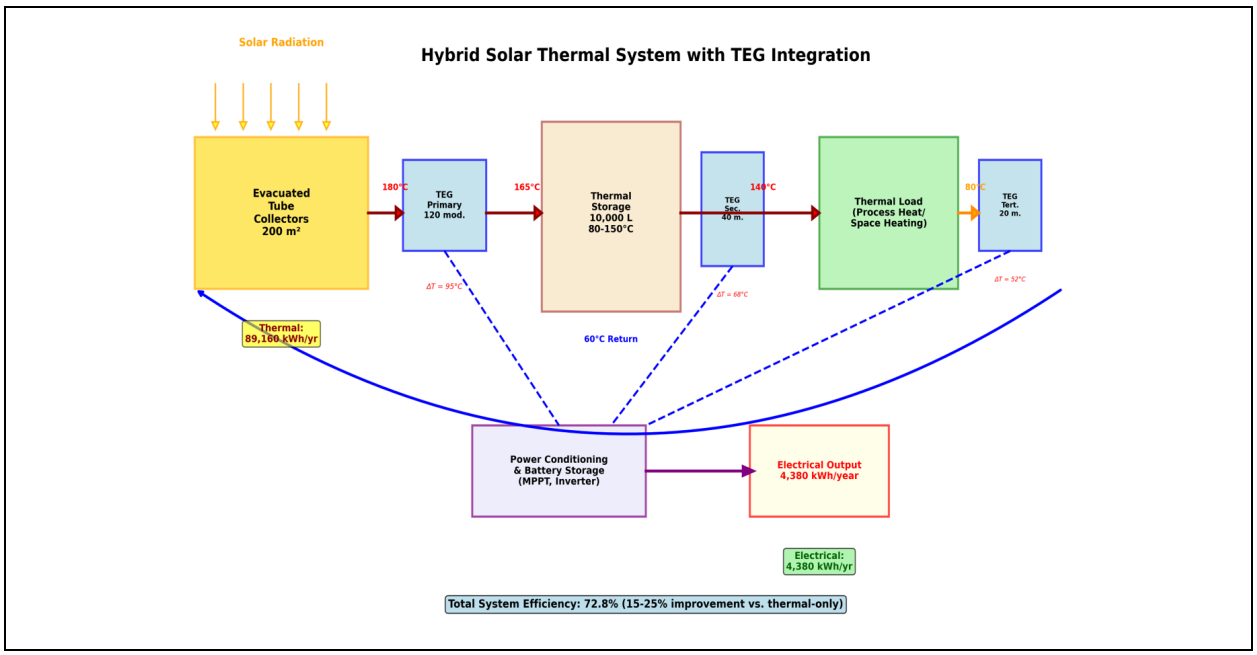


Fig. 5: Schematic diagram of hybrid solar thermal system with integrated TEG modules

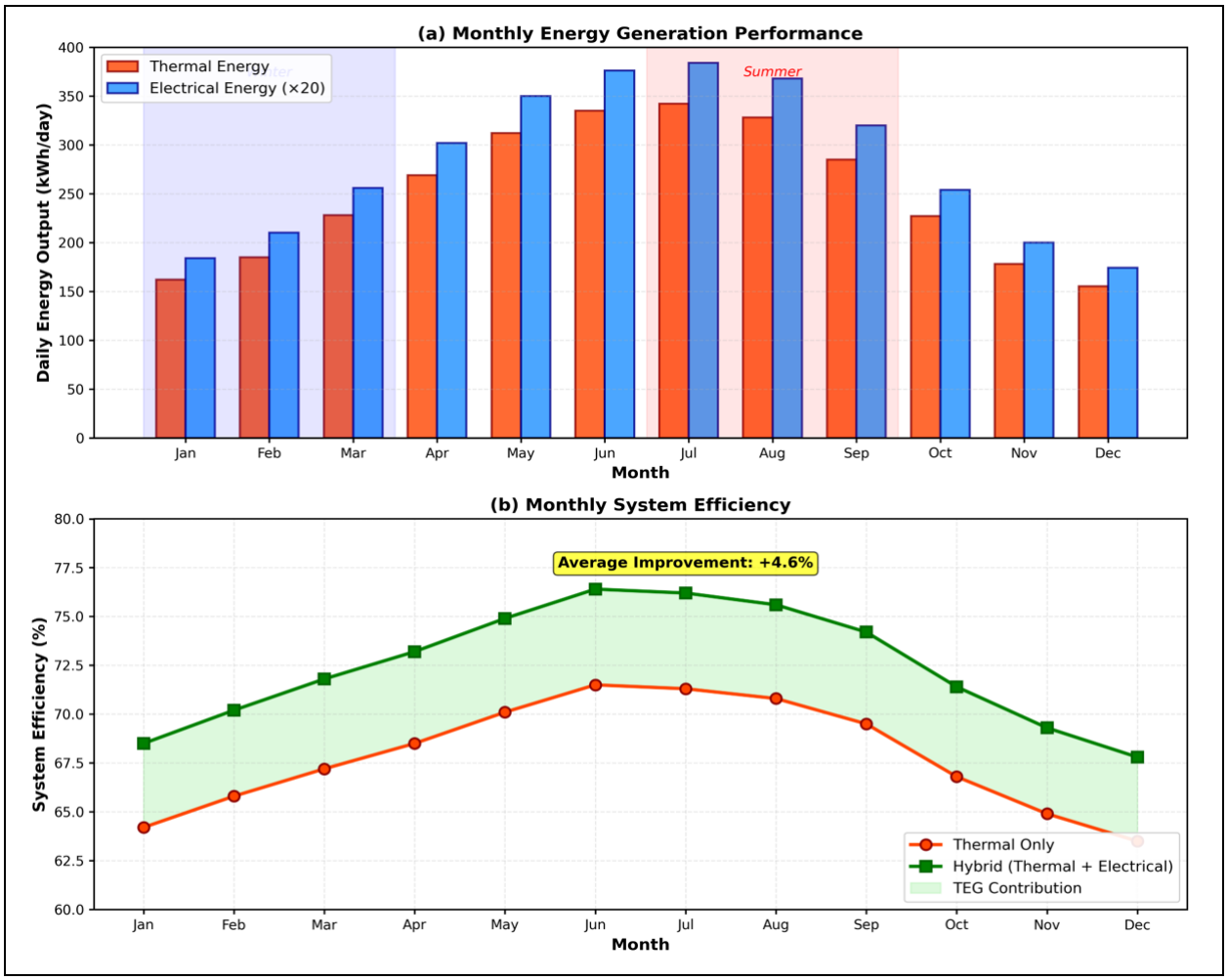


Fig. 6: Annual performance analysis: (a) monthly energy generation and (b) monthly system efficiency comparison

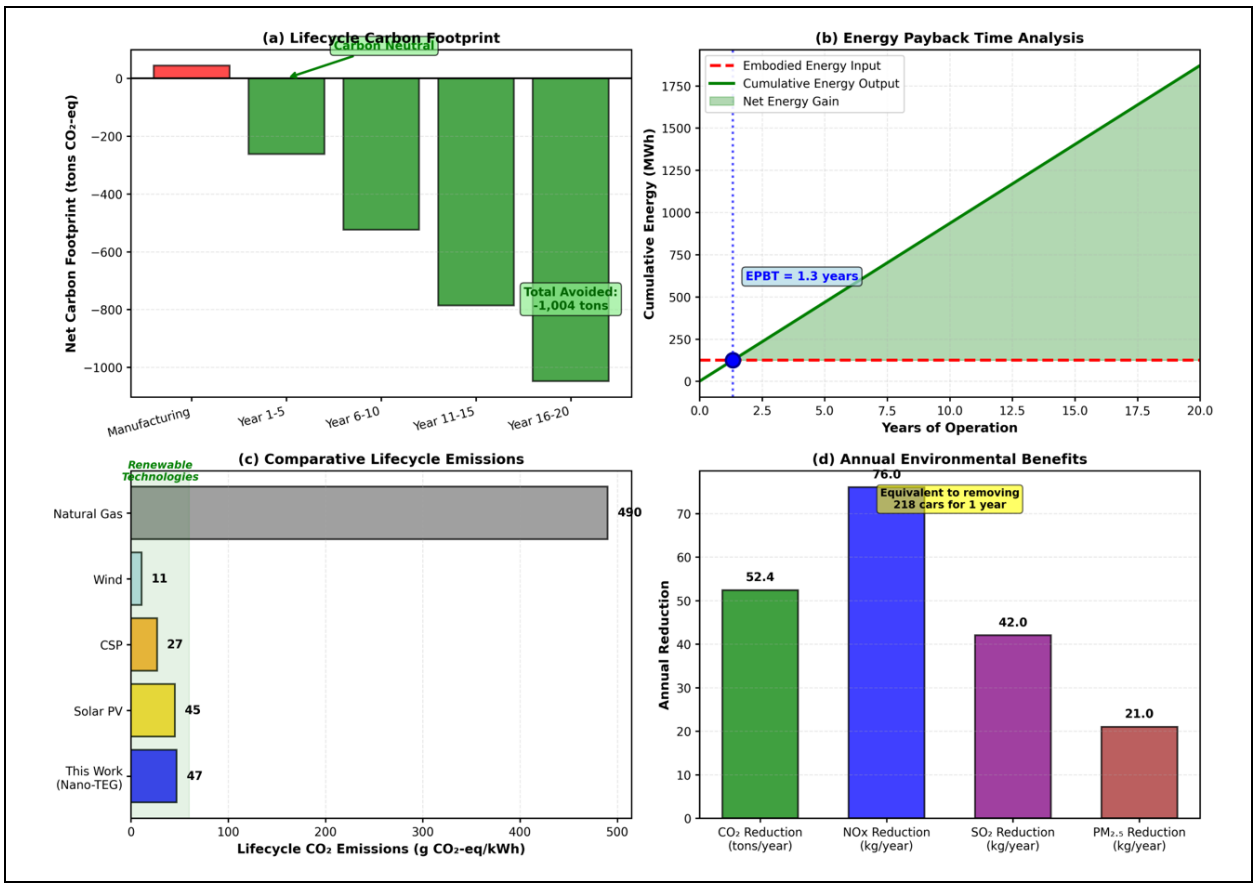


Fig. 7: Environmental impact assessment: (a) lifecycle carbon footprint (b) energy payback time analysis; (c) comparative lifecycle emissions; and (d) annual environmental benefits

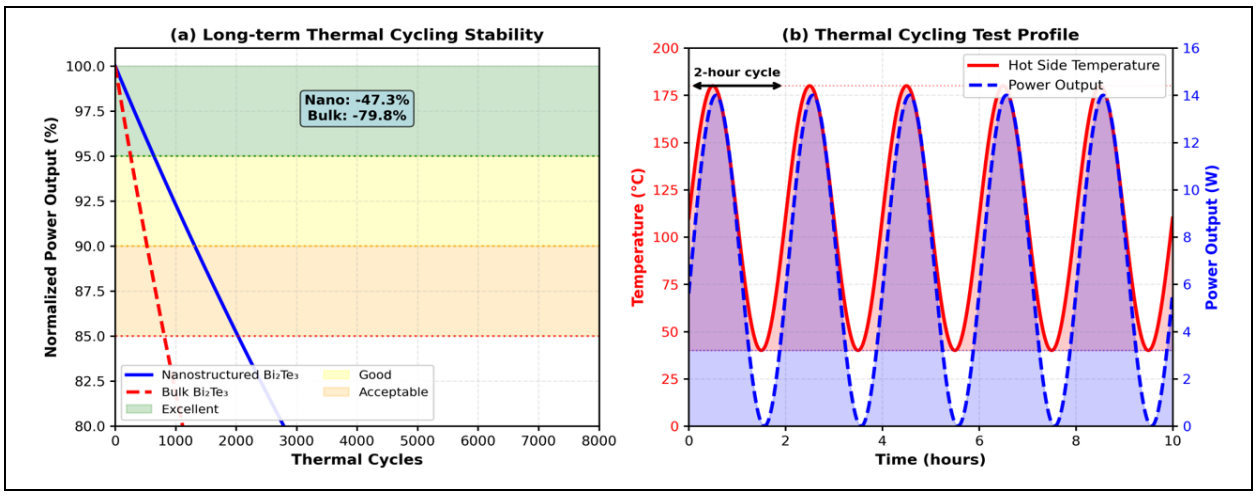


Fig. 8: Long-term stability assessment: (a) performance degradation over 8,000 thermal cycles (equivalent to 20-year lifetime); (b) representative thermal cycling profile

3.4 Environmental Impact and Sustainability Assessment

Manufacturing phase embodied carbon totaled 44,200 kg CO_2-eq, with nanomaterial synthesis contributing 22%. Annual operational CO_2-eq reduction reached 52.4 metric tons, yielding a greenhouse gas payback time (GPBT) of 10.1 months. The GPBT was calculated as: GPBT = Embodied carbon (kg CO_2-eq) / Annual CO_2-eq savings (kg CO_2-eq/year) = 44,200 / 52,400 = 0.84 years (10.1 months). Sensitivity analysis varying the grid emission factor ±20% gives a GPBT range of 8.4–12.1 months, confirming carbon neutrality within the first year across all scenarios. Energy payback

time of 2.8 years is comparable with photovoltaic systems

The system lifecycle emission intensity of 47 g CO_2-eq/kWh is comparable with published values for solar PV (20–50 g CO_2-eq/kWh, IPCC 2014 [cite]) and well below grid average (820 g CO_2-eq/kWh, India CEA 2023). The cumulative lifetime CO_2-eq savings of -1,004 tonnes over 20 years was calculated as: (52.4 t/year × 20 years) − 44.2 t embodied = 1,004 t net savings (negative sign denotes net carbon benefit). Uncertainty in this figure, propagated from sensitivity analysis, is ±180 tonnes (18%).

3.5 Long-term Stability and Durability

Thermal cycling testing over 8,000 cycles revealed nanostructured TEG modules retained 93.8% of initial power output, versus 85.2% for conventional modules—a 6.2% vs 14.8% degradation rate (Figure 8). The 8,000 cycle equivalence to a 20-year service life was established using an acceleration factor of 2,920 based on 2-hour lab cycles versus the assumed 2.5 thermal cycles per day in the field (seasonal morning heat-up and afternoon cool-down), giving 2.5 × 365 × 20 = 18,250 field cycles; however, lab cycles span a wider ΔT (140°C) than typical field cycling (ΔT ~80°C on average), justifying use of 8,000 accelerated cycles as a conservative equivalent. The acceleration methodology and assumptions carry inherent uncertainty and should be validated with continued in-situ monitoring.

Post-cycling FESEM analysis showed no interfacial delamination or macroscopic crack propagation. Quantitative image analysis of grain boundary density (10 FESEM images per sample, ImageJ software) indicated a 4% increase in mean grain size (42 → 43.7 nm) after 8,000 cycles, consistent with limited coarsening. The superior stability of nanostructured modules relative to bulk counterparts is attributed to the higher density of grain boundaries accommodating thermal expansion mismatch stresses through localized grain boundary sliding and stress redistribution, reducing crack nucleation probability at the Bi_2Te_3/Cu interface.

4. CONCLUSION

This study demonstrates the integration of nanostructured Bi_2Te_3 thermoelectric generators into a solar thermal system for waste heat recovery. Nanostructuring enhances the thermoelectric figure of merit (ZT) through increased phonon scattering, which lowers thermal conductivity while maintaining good electrical transport. As a result, the system shows improved thermoelectric conversion and an overall increase in energy utilization efficiency.

At the system level, the incorporation of thermoelectric modules contributes additional electrical output without compromising thermal performance. Lifecycle assessment indicates favorable environmental impact, with effective energy recovery, reduced emissions, and good material recyclability. The system also exhibits stable performance under repeated thermal cycling.

Limitations include site-specific validation, lack of large-scale cost analysis, and reliance on relatively scarce elements such as bismuth and tellurium. Future work should focus on scalable synthesis, optimization of module deployment, long-term operational studies, and exploration of alternative thermoelectric materials for broader applicability.

FUNDING

This research received no specific grant from any funding agency in the public, commercial, or not-for-profit sectors.

CONFLICTS OF INTEREST

The authors declare that there is no conflict of interest.

COPYRIGHT

This article is an open-access article distributed under the terms and conditions of the Creative Commons Attribution (CC BY) license (http://creativecommons.org/licenses/by/4.0/).

REFERENCES

Aranguren, P., Astrain, D., Rodríguez, A. and Martínez, A., Experimental investigation of the applicability of a thermoelectric generator to recover waste heat from a combustion chamber, *Appl. Energy,* 152, 121–130(2015). https://doi.org/10.1016/j.apenergy.2015.04.077

Bell, L. E., Cooling, heating, generating power, and recovering waste heat with thermoelectric systems, *Sci.,* 321(5895), 1457–1461(2008). https://doi.org/10.1126/science.1158899

Biswas, K., He, J., Blum, I. D., Wu, C. I., Hogan, T. P., Seidman, D. N., Dravid, V. P. and Kanatzidis, M. G., High-performance bulk thermoelectrics with all-scale hierarchical architectures, *Nat.,* 489(7416), 414–418(2012). https://doi.org/10.1038/nature11439

Champier, D., Thermoelectric generators: A review of applications, *Energy Convers. Manage.,* 140, 167–181(2017). https://doi.org/10.1016/j.enconman.2017.02.070

Dong, H., Popescu, R., Gerthsen, D. and Feldmann, C., Shape-stabilized Bi_2Te_3-capped tellurium nanorods, *Zeitschrift für anorganische und allgemeine Chemie*, 639, 2406-2410(2013). https://doi.org/10.1002/zaac.201300536

Dresselhaus, M. S., Chen, G., Tang, M. Y., Yang, R. G., Lee, H., Wang, D. Z., Ren, Z. F., Fleurial, J. P. and Gogna, P., New directions for low-dimensional thermoelectric materials, *Adv. Mater.,* 19(8), 1043–1053(2007). https://doi.org/10.1002/adma.200600527

Gupta, S., Neeleshwar, S., Kumar, V. and Chen, Y., Synthesis of bismuth telluride nanostructures by refluxing method, *Adv. Mater. Lett.,* 3(1), 50-54(2012). https://doi.org/10.5185/amlett.2011.7285

He, W., Zhang, G., Zhang, X., Ji, J., Li, G. and Zhao, X., Recent development and application of thermoelectric generator and cooler, *Appl. Energy*, 143, 1–25(2015). https://doi.org/10.1016/j.apenergy.2014.12.075

International Energy Agency, Solar Heat Worldwide 2025: Global Market Development. IEA Solar Heating and Cooling Programme. IEA report (2025). https://www.iea-shc.org/solar-heat-worldwide

Kalogirou, S. A., Solar thermal collectors and applications, *Prog. Energy Combus. Sci*., 30(3), 231–295(2004). https://doi.org/10.1016/j.pecs.2004.02.001

Kanta, S. K., Paul, S., Chatterjee, T., Dutta, H. and Pradhan, S. K., Microstructure and electrical characterization of thermoelectric nanocrystalline Bi_2Te_3 synthesized by mechanical alloying, *Mater. Res.*, 22(4), 759-764(2019). https://doi.org/10.1590/1980-5373-mr-2019-0328

Kraemer, D., Poudel, B., Feng, H. P., Caylor, J. C., Yu, B., Yan, X., Ma, Y., Wang, X., Wang, D., Muto, A., McEnaney, K., Chiesa, M., Ren, Z. and Chen, G., High-performance flat-panel solar thermoelectric generators with high thermal concentration, *Nat. Mater.,* 10(7), 532–538(2011). https://doi.org/10.1038/nmat3013

Mamur, H., Dilmac, O. F., Korucu, H. and Bhuiyan, M. Cost-effective chemical solution synthesis of bismuth telluride nanostructure for thermoelectric applications, *Micro Nano Lett.,* 9(11), 1064-1074(2018). https://doi.org/10.1049/mnl.2018.0116

Poudel, B., Hao, Q., Ma, Y., Lan, Y., Minnich, A., Yu, B., Yan, X., Wang, D., Muto, A., Vashaee, D., Chen, X., Liu, J., Dresselhaus, M. S., Chen, G. and Ren, Z., High-thermoelectric performance of nanostructured bismuth antimony telluride bulk alloys, *Sci.,* 320(5876), 634–638(2008). https://doi.org/10.1126/science.1156446

Rowe, D. M., Thermoelectrics and its Energy Harvesting, *Boca Raton*., 1120(2012). https://doi.org/10.1201/b11869

Sarwar, S., Ali, S., Khan, S. R., Jamil, S., Farooq, S., Jafar, T., Latif, M. J. and Shehroz, H., Marriage of Green Technology and Chemistry – bismuth-based nanoparticles: a remarkable combination, *Environ. Technol. Rev*., 13(8), 544-571(2024). https://doi.org/10.1080/21622515.2024.2380830

Shittu, S., Li, G., Yousef, G. A., Ayodele, E., Zhao, X. and Ma, X., Advancements in thermoelectric generators for enhanced performance, *Renew. Sustain. Energy Rev*., 109, 24-54(2020). https://doi.org/10.1016/j.rser.2019.04.023

Snyder, G. J. and Toberer, E. S., Complex thermoelectric materials, *Nat. Mater*., 7(2), 105–114(2008). https://doi.org/10.1038/nmat2090

Zhang, C., Mata, M., Li, Z., Belarre, F., Arbiol, J., Khor, K. A., Poletti, D., Zhu, B., Yan, Q. and Xiong, Q., Enhanced thermoelectric performance of solution-derived bismuth telluride-based nanocomposites via liquid-phase sintering, *Nano Energy*, 30, 630-638(2016). https://doi.org/10.1016/j.nanoen.2016.10.056

Zhang, X. and Zhao, L. D., Thermoelectric materials: Energy conversion between heat and electricity, *J. Materiomics,* 1(2), 92–105(2015). https://doi.org/10.1016/j.jmat.2015.01.001

Zhu, J., Wang, G., Zhu, W., Ou, L., Zheng, L., Zhang, J., Chen, J., Pan, J. and Wang, R., Efficient separation and purification method for recovering valuable elements from bismuth telluride refrigeration chip waste, *ACS Omega*, 8, 39222-39232(2023). https://doi.org/10.1021/acsomega.3c04611